Laser Assist Scattering with Lennard-Jones Screening Potential for Ar-Atom

[1]Kant Prasad Thapa, [2,3]Saddam Husain Dhobi, [1]Kamal Shrestha, [1]Topendra Budha, [1]Lalmani Acharya, [1]Topendra Dangi [2]Subarna Budhathoki, [1,3]Kishori Yadav, [1,3]Suresh Prasad Gupta

[1]Department of Physics, Patan Multiple Campus, Tribhuvan University, Patandhoka, Lalitpur, Nepal
[2]Central Department of Physics, Tribhuvan University, Kirtipur, Kathmandu, Nepal
[3]Innovative Ghar Nepal, Lalitpur, Nepal
Corresponding Author: saddam@ran.edu.np /thapakant28@gmail.com

Abstract: The objective of this work is to study the laser-assisted electron-Argon scattering. For this authors design screening Lennard-Jones Potential and develop mathematical model to study the DCS with photon energy, momentum and scattering angle. The differential cross section (DCS) nature was study using online MATLAB student package with various influencing parameters. Notably, the DCS for the first-order Bessel function exhibits higher values than its zero-order counterpart, owing to the unique attributes of Bessel functions. The first order introduces amplitude modulation, triggering phase shifts and constructive interference, resulting in elevated DCS values. Moreover, the interplay of screening parameters, laser field strength, and momentum changes significantly influences scattering behavior. Higher screening reduces particle interaction, yielding decreased DCS, while lower screening intensifies scattering, leading to higher DCS values. These findings provide crucial insights into the underlying physics of these interactions, offering valuable guidance for interpreting experimental results and understanding particle behavior in this specific context.

Keywords: Laser assist, scattering, Screening Lennard-Jones, Scattering angle, differential cross section, Bessel function

Introduction

The Laser-assisted electron scattering (LAES) in condensed phase particle densities, using nano-structured systems in superfluid He (thickness: 32–340 Å). Free electrons generated by strong-field ionization gain significant energy through multiple LAES processes. This introduces new avenues for solid-state and liquid-phase electron dynamics studies [1]. The examines electron-nucleon scattering with and without a circularly polarized electromagnetic pulse. The research calculates the differential cross section (DCS) using the Dirac-Volkov formalism and makes two comparisons: DCS in the absence and presence of the laser field, and electron-proton vs. electron-neutron scattering with laser effects. Findings indicate reduced DCS with the laser field. Additionally, the electric form factor decreases with increased electron energy in electron-proton scattering but increases in electron-neutron scattering. Notably, the study doesn't involve screening parameters. Moreover, the form factors for both scattering situations are unchanged by raising the laser field strength up to 10^8V/cm [2].

The theoretically analyzes electron-proton scattering with initially spin-polarized electrons under a circularly polarized electromagnetic field. It employs the first-Born approximation and Dirac-Volkov states to derive a differential cross-section expression. The impact of the electromagnetic field on electron polarization and spin is examined. Notably, the research doesn't incorporate screening parameters [3]. The electroweak theory to analyze elastic scattering, considering circularly polarized laser fields. Using Dirac-Volkov wave functions in the first-Born approximation, the differential cross-section is derived. Results highlight the superiority of electroweak theory over Fermi approximation for high-energy interactions. The laser's strength and frequency significantly impact photon exchange, linked to Bessel functions in calculations. Importantly, screening parameters were not utilized in this study [4].

The introduces an apparatus to measure kinetic energy and angular distributions of femtosecond laser-assisted electron scattering (LAES) signals with high efficiency. It includes an ultrashort pulsed electron gun, gas injection nozzle, time-of-flight analyzer, and a sensitive electron detector. An analysis method is established to extract this information from raw data. Experimental results with Ar atoms in a near-infrared laser field demonstrate a 40-fold increase in detection efficiency compared to prior work in 2010. Importantly, screening parameters were not part of this study [5]. The presents a stable random laser formed from Rhodamine 6G dye-infused ZnO@C-N microstructures, achieved via stimulated Raman scattering and random lasing coupling. Raman peaks act as seeds, amplified by elastic scattering in the disordered medium. ZnO@C-N structures with abundant nanosheets enhance scattering. This enables operation with low scatterer concentration (as low as 2mg/ml). The research demonstrates stable and reproducible Raman modes, unaffected by pulse-to-pulse pump energy variations. The findings offer a novel method for wavelength tuning in random lasers, with potential for practical applications and laser mode selection [6]. Notably, screening parameters were not considered in this study.

The image classification methods on simulated cell model patterns to advance label-free cytometry. Simulation factors encompass mitochondria count, surface texture, laser wavelength, and viewing angle [7]. Notably, screening parameters were not incorporated in their research. The study investigates laser-assisted (e,2e) ionizing collisions in hydrogen at moderate laser intensities and photon energies beyond the soft-photon approximation. It employs Gordon-Volkov wave functions for nonperturbative treatment of electron interactions with the laser field. The atomic dressing is addressed with first-order perturbation theory. The research provides a closed-form formula for the nonlinear triple differential cross section (TDCS), applicable for linear and circular polarizations. Analytical expressions in the weak field and low-photon energy regimes are derived. Notably, screening parameters were not considered in this work [8].

The investigates enhancing antihydrogen production, crucial for the GBAR experiment, through laser-mediated charge-exchange in positronium-antiproton collisions. A perturbative approach combines Coulomb-Born approximation for collisions and first-order perturbation theory for laser-atom interactions. Laser parameters (wavelength and intensity) are extensively studied within experimental constraints, indicating potential for significantly increased antihydrogen production under specific irradiation conditions. Notably, screening parameters were not part of this study [9]. LJP studies are crucial for understanding the differential cross section of shielding materials, as atomic binding-induced scattering significantly impacts radiation shielding. Materials with optimal wavelength and bond length are considered excellent shields, absorbing and safeguarding against various radiation hazards. Additionally, LJP contributes to scattering by redirecting radiation when it encounters two atoms. Photon interaction within the potential field

is a key aspect of scattering, providing valuable insights into energy, momentum, differential cross section, and particle formation [10,11].

The analyzing Lennard-Jones Potential (LJP) interactions among various atoms and molecules. A mathematical model is developed and implemented in MATLAB to examine LJP direct correlation functions. Interactions like carbon-carbon, carbon-oxygen, oxygen-oxygen, and others are studied. Results reveal specific LJP values and distances for different interactions, providing insights valuable for molecular physics, computational chemistry, and molecular modeling research [12]. Notably, screening parameters were not employed in this work. Material physics models often rely on atomic interaction potentials, describing phenomena like phase transitions and diffusion. Parameters are derived from thermodynamic properties and crystal structure, aligning simulations with experiments. Pair potentials, though simplified, serve as practical foundations for more complex models, validated through real-world simulations [13]. This potential is increasingly used to determine the intermolecular parameters for simple molecules (H_2, O_2, N_2, CO, CH_4), in which we add the inter-action terms in some cases potential iodide(KI) molecule [14].

$$V = 4\epsilon_{ij} \left[\left(\frac{\sigma_{ij}}{r_{ij}} \right)^{12} - \left(\frac{\sigma_{ij}}{r_{ij}} \right)^{6} \right] \tag{1}$$

r_{ij}=Internuclear separation, σ_{ij} =equilibrium distance and ϵ_{ij}=binding energy.

In a linearly polarized laser beam, high scattering energy and moderate field intensities affect inelastic electron-H(2s) dispersion. Different initial and final states distinguish it from elastic scattering. Absorption of one photon excites metastable hydrogen. Accurate mathematical treatment involves complex considerations, including the Gordon-Volkov wave function and first-order perturbation theories. The first Born approximation is used to model hydrogen atom interaction with fast projectiles [15]. Yadav et al. discovered that the differential scattering cross - sectional area reduces with an increase in scattering angle. The elastic scattering amplitude determines the differential scattering cross - sectional area for the electric field parallel to the axis of momentum transfer. Finally, it was found that the polarization of the laser field has a significant impact on the differential scattering cross section [16].

In the instance of inelastic scattering, Dhobi et al. investigate the differential cross-section in the presence of a low laser field (visible and UV). The theoretically developed model predicts that as the target absorbs the energies, the differential cross section grows. When the target emits energy, the differential cross-section initially drops to a minimum and eventually reaches its maximum value. At 5 eV, 10 eV, 13 eV, 16 eV, 20 eV, 25 eV, and 30 eV, energy emission takes place. Additionally, the differential cross-section grows as the scattering angle increases [17]. Yadav et al study the DCS with a coulomb potential in elliptically polarized beam with single photon absorption and found Less than the differential cross - sectional area obtained by Flegel et al. (2013), which is roughly $10^{-17}m^2$, the numerically computed differential cross section in the research is between $10^{-19}m^2$ to $10^{-20}m^2$ [18].

Motivation

The research gap identified in this context revolves around the absence of a comprehensive study on the scattering behavior of particles in the presence of a laser field, particularly when considering the screening effects of the Lennard-Jones potential. While there is a substantial body of research dedicated to laser-assisted scattering involving various target entities (such as atoms, molecules, electrons, and protons), few studies have incorporated the crucial aspect of

screening parameters. This gap is significant due to the critical role that screening effects play in systems involving a multitude of electrons and protons, or in many-body problem scenarios. The present work aims to address this deficiency by introducing and analyzing the screening effect between two atoms/molecules, utilizing a modified classical Lennard-Jones potential as the screening function for the study. This research aims to provide valuable insights into the behavior of particles in laser-assisted scattering, shedding light on the intricate interplay between screening effects and the underlying potential.

Significant

The research addresses a critical gap in the study of scattering behavior in the presence of a laser field, specifically considering the screening effects of the Lennard-Jones potential. It highlights the significance of understanding interactions between electrons, atoms, and molecules within systems exposed to both mono- and non-monochromatic spectra. These interactions are profoundly affected by screening factors generated by the presence of electrons. The findings not only advance fundamental knowledge in quantum dynamics but also hold promise for practical applications in materials science, chemistry, and technology development. Recommendations include further investigations into multi-particle quantum dynamics, expanding laser-assisted scattering studies, and fostering interdisciplinary collaborations to tackle complex problems.

Methodology

The differential cross section is

$$\frac{d\sigma}{d\Omega} = \frac{k_f}{k_i}\left(\frac{4m\pi^2}{\hbar^2}\right)^2 |T_{fi}|^2 \tag{2}$$

The quantum free-free differential cross - sectional area can be determined if the T matrix for free-free transitions is discovered. We examine the connection between the S and the T matrices in order to determine the T matrix.

$$S_{fi} = \delta_{fi} - i2\pi\delta(E_f - E_i)\ T_{fi} \tag{3}$$

Now, S matrix for free-free scattering

$$S_{fi} = \delta_{fi} - \frac{i}{\hbar}\int\int_{-\infty}^{+\infty}\langle X_f(r,t')|V(r)|\Psi_i(r,t')\rangle dt' \tag{4}$$

where X (r, t) denotes the wave function for an electron connected to an external electromagnetic field and Ψ (r, t) denotes the wave function for an electron coupled to an external electromagnetic field while also being in the existence of a scattering potential V (r). The Schrodinger time-dependent equation's wave function [19] is

$$X(r,t) = 1\frac{1}{(2\pi)^{3/2}} exp\{i\frac{p}{h}\cdot(r + \frac{e}{m}\int A(t')dt' - i\frac{E}{\hbar}t$$
$$- i\frac{e^2}{2m\hbar}\int A^2(t')dt' \tag{5}$$

Equation (5) is Volkov wave function, E is the free electron's kinetic energy. Keep in mind that the momentum operator's eigenvalue is $\hat{\boldsymbol{p}}$. The Volkov wave function's general form is given by equation (5) is obtained with vector potential as shown in equation (6)

$$X(r,t) = \frac{1}{(2\pi)^{\frac{3}{2}}} exp \left\{ -\frac{i}{\hbar}\left(E + \frac{e^2 a^2}{4m}\right)t + i\frac{\boldsymbol{p}}{\hbar} \cdot \left(\boldsymbol{r}\frac{e\,\boldsymbol{a}}{m\omega} sin(\omega t)\right) - \right.$$

$$\left. i\frac{e^2 a^2}{8m\hbar\omega} sin(2\omega t)\right\} \tag{6}$$

This equation explain the wave function of electrons in a laser field.

$$S_{fi} = \delta_{fi} - \frac{i}{\hbar}\int_{-\infty}^{+\infty}\langle X_f(r,t)|V(r)|\Psi_i(r,t)\rangle dt' \tag{7}$$

Using the first Born approximation, let's calculate the time integral by supposing that the scattered potential is low.

$$\int_{-\infty}^{+\infty}\langle X_f(r,t)|V(r)|X_i(r,t)\rangle dt' = \frac{1}{(2\pi)^3}\frac{i}{\hbar}\int_{-\infty}^{+\infty}e^{i(E_f - E_i)t'/\hbar}\,dt'$$

$$\times \int_{-\infty}^{+\infty}exp\left\{-i\frac{e}{m\hbar\omega}\boldsymbol{Q}\cdot\boldsymbol{a}\,sin(\omega t)\right\}dt'$$

$$\times \int V(\boldsymbol{r})e^{-i(\boldsymbol{Q}\cdot\,\boldsymbol{r})/\hbar}d^3\,r' \tag{8}$$

When the momentum transfer formula $\boldsymbol{Q} = \boldsymbol{p_f} - \boldsymbol{p_i}$ was utilized. Lets use the three major relationships to continue: Scattering amplitude of the first born approximation,

$$f_{Born}{}^{(1)} = -\frac{m}{2\pi\hbar^2}\int V(r)e^{-iQ\cdot\frac{r}{\hbar}}d^3 r \tag{9}$$

Where screening Lennard-Jones potential $V(r) = 4\epsilon\left[\left(\frac{\sigma}{r}\right)^{12} - \left(\frac{\sigma}{r}\right)^6\right]e^{-\eta r}$ Function's inverse Fourier transform [20]. Now, the S matrix can be expressed from above for the nth element.

$$S_{fi} = \delta_{fi} - i2\pi\delta(E_f - E_i + n\hbar\omega)\left[-\frac{1}{(2\pi)^3}\frac{2\pi\hbar^2}{m}J_n\left(-\frac{e}{m\hbar\omega}(\boldsymbol{Q}\cdot\boldsymbol{a})\right)f_{Born}^1\right] \tag{10}$$

Comparing equation (10) with standard scattering matrix equation the recognizing T_{fi} matrix is obtained as,

$$T_{fi} = -\frac{1}{(2\pi)^3}\frac{2\pi\hbar^2}{m}J_n\left(-\frac{e}{m\hbar\omega}(\boldsymbol{Q}\cdot\boldsymbol{a})\right)\,f_{Born}^1 \tag{11}$$

Where, $f_{Born} = \frac{16\epsilon\pi\hbar}{iq}\left[-\frac{\sigma^{11}(\eta+iq)^{10}}{3628800} + \frac{\sigma^{11}(\eta-iq)^{10}}{3628800} + \frac{\sigma^5(\eta+iq)^4}{24} - \frac{\sigma^5(\eta-iq)^4}{24}\right]$. Now the DCS is obtained in a.u. term as

$$\frac{d\sigma_{FF}^n}{d\Omega} = \frac{k_f}{k_i}\left|J_n\left(-\frac{e}{m\hbar\omega}(\boldsymbol{q}\cdot\boldsymbol{a})\right)f_{Born}^1\right|^2 \tag{12}$$

Also for zero order Bessel function, $J_0 = 1$, for first order Bessel function $J_1 = -\frac{qacos\theta}{2\omega}$ and the DCS for thes two Bessel function is shown in figure (13) and (14), respectively.

$$\left(\frac{d\sigma}{d\Omega}\right)_{J_0} = \frac{k_f}{k_i}|f_{Born}|^2 \tag{13}$$

$$\left(\frac{d\sigma}{d\Omega}\right)_{J_1} = \frac{k_f}{k_i}\left(\frac{qa\cos\theta}{2\omega}\right)^2 |f_{Born}|^2 \tag{14}$$

Results and Discussion

DCS for First order Bessel Function in Lennard-Jones Screening Potential

The Developed equation was computed using MATLAB online student package. The equation nature of equation (13) is with different parameters are shown in figure 1 to 3 while equation (14) are shown in figure 4 to 6. The laser field strength is taken 10^8V/cm, the energy of laser photon is 1.17 eV, the screening parameters value ranges from 0.1 to 0.9. The DCS with scattering angle is shown in figure 1. The Differential Cross Section (DCS) exhibits a minimum value at a scattering angle of zero. This phenomenon can occur due to the particles involved may experience a configuration or alignment that minimizes their mutual interaction or interference. Additionally, influenced by the specific properties of the particles, the nature of the scattering potential, or the presence of external factors like a laser, which could introduce screening effects or alter the scattering behavior.
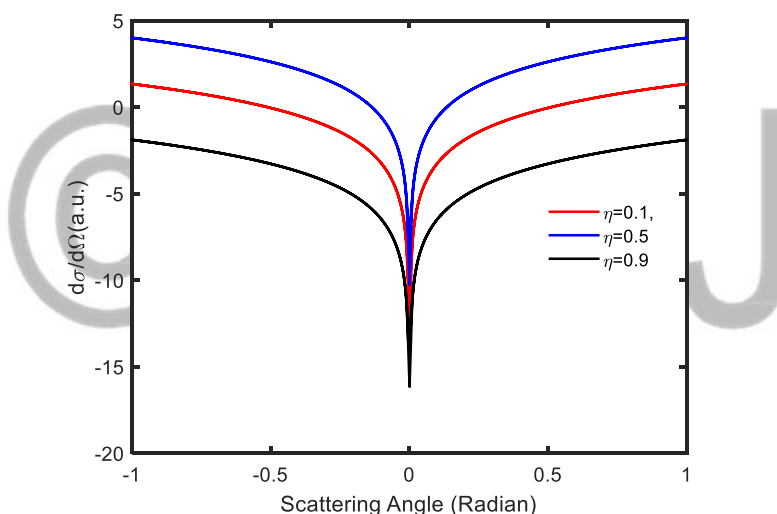
Figure 1: Scattering angle vs DCS in laser field

The decrease in the Differential Cross Section (DCS) with decreasing scattering angle can be attributed to the fundamental principles of scattering phenomena. As the scattering angle decreases, it implies that the particles are more likely to be scattered in the forward direction. At very small scattering angles, the deflection or change in trajectory of the particles is minimal. This indicates that the interaction potential between the particles and the target is such that they tend to move predominantly in their original direction. Also, the particles are less likely to experience significant interference or mutual repulsion, which can lead to a decrease in scattering. This may be due to a screening effect, where other charges in the environment reduce the effective interaction between the particles.

The observed DCS can be also explained by considering the interplay of screening parameters, the laser field, and their effects on the scattering process. When the screening effect is higher, it means that the interaction between particles is effectively reduced due to the presence of other charges. In a stronger screening environment, the particles experience less mutual repulsion,

which can lead to a decrease in scattering. This reduction in scattering is reflected in the lower DCS observed in a laser field with higher screening effect.

Conversely, in a situation with lower screening parameters, the interaction between particles is less mitigated, leading to a stronger scattering tendency. This results in a higher DCS. The presence of the laser field can further influence the scattering process. A laser can alter the energy states and behavior of the particles, potentially leading to different scattering outcomes.
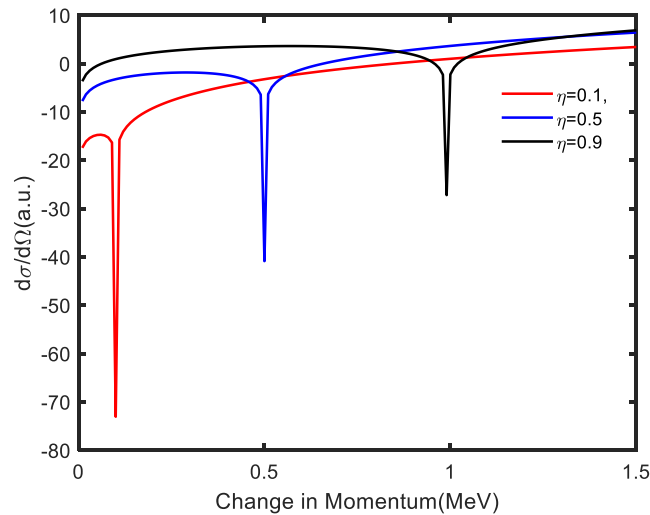
Figure 2: Change in momentum of electron vs DCS

The observed trend in Figure 2, where the DCS decreases and reaches a minimum for the considered screening parameters, can be attributed to the interplay of screening effects and momentum changes of the incident particles. Higher screening parameters imply a stronger reduction in the interaction between charged particles due to the presence of other charges. This results in a decrease in scattering, which is reflected in the lower DCS. When the momentum of the incident particle changes, it can influence the nature of the interaction with the target particles. In scenarios with higher screening, the particles are less likely to experience significant interference or mutual repulsion even with a change in momentum, leading to a higher DCS. On the other hand, in situations with lower screening parameters, the interaction between particles is less mitigated, causing a stronger scattering tendency, resulting in a lower DCS. Furthermore, the DCS of higher screening being higher and lower screening being lower with changes in momentum underscores how screening parameters play a crucial role in modifying the scattering behavior. It's essential to consider these parameters alongside the momentum changes to gain a comprehensive understanding of the scattering process in this specific context.
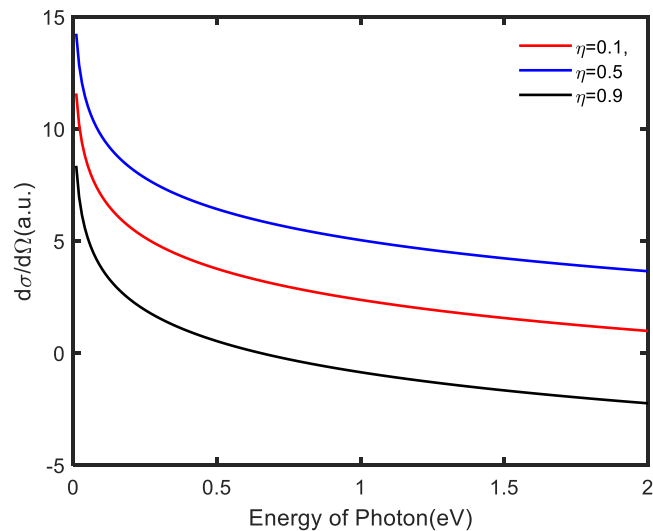
Figure 3: Energy of Photon vs DCS

The observed trend the DCS decreases with an increase in the energy of the laser field can be attributed to the way higher energy photons from the laser interact with the particles in the scattering process. Higher energy photons can induce transitions in the energy states of the particles, potentially leading to a reduction in scattering events and, consequently, a lower DCS. Moreover, when comparing the DCS for higher screening effect to lower screening effect, the finding that higher screening effect results in a lower DCS suggests that the presence of additional charges in the higher screening environment reduces the effective interaction between the particles. This reduction in interaction leads to a decrease in scattering events, ultimately yielding a lower DCS. In contrast, lower screening effect implies that the particles experience less mitigation of their mutual interaction, which can result in a stronger scattering tendency. This leads to a higher DCS in scenarios with lower screening effect. The interplay between the energy of the laser field, screening effect, and their respective impacts on the scattering process provides valuable insights into the underlying physics governing these interactions. Understanding these dynamics is crucial for interpreting experimental results and gaining deeper insights into the behavior of particles in this specific context.

DCS for First order Bessel Function in Lenard-Jones Screening Potential

The figures presented in the study illustrate the behavior of the Differential Cross Section (DCS) with respect to different parameters: laser photon energy (Figure 4), scattering angle (Figure 5), and electron momentum change (Figure 6). Notably, the DCS for the Bessel first order exhibits higher values compared to the zero order. This intriguing observation can be attributed to the distinctive characteristics of Bessel functions. The zero order Bessel function represents oscillations without amplitude modulation, whereas the first order exhibits oscillations with one amplitude modulation. In the context of scattering, this translates to distinct patterns of particle dispersion. The amplitude modulation in the first-order Bessel function introduces phase shifts and interference patterns, potentially leading to constructive interference in specific directions. This, in turn, results in higher DCS values. Moreover, the mathematical structure of Bessel functions, particularly the presence of amplitude modulation in the first order, inherently gives rise to differing scattering patterns compared to the zero order. Depending on the underlying physics of the specific phenomena being studied, the amplitude modulation introduced by the first-order Bessel function may align more accurately, resulting in the observed higher DCS values. In essence, the discrepancy in DCS between the first and zero order Bessel functions

arises from the nuanced mathematical and physical traits associated with each, ultimately influencing the scattering outcomes in distinct ways.
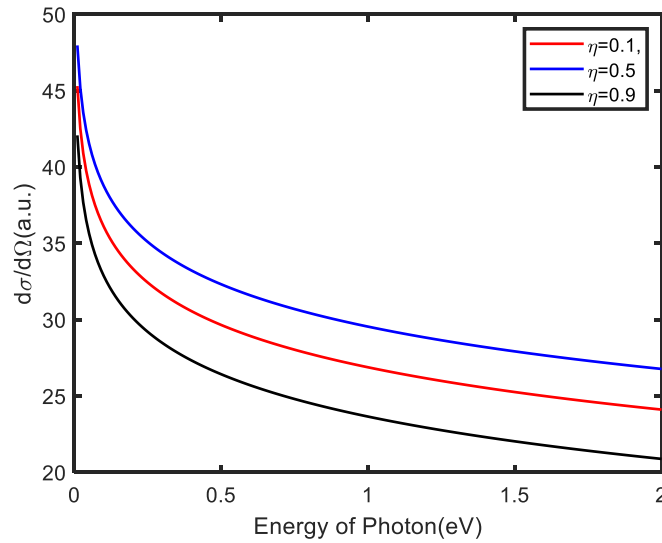
Figure 4: Photon energy vs DCS First order Bessel function
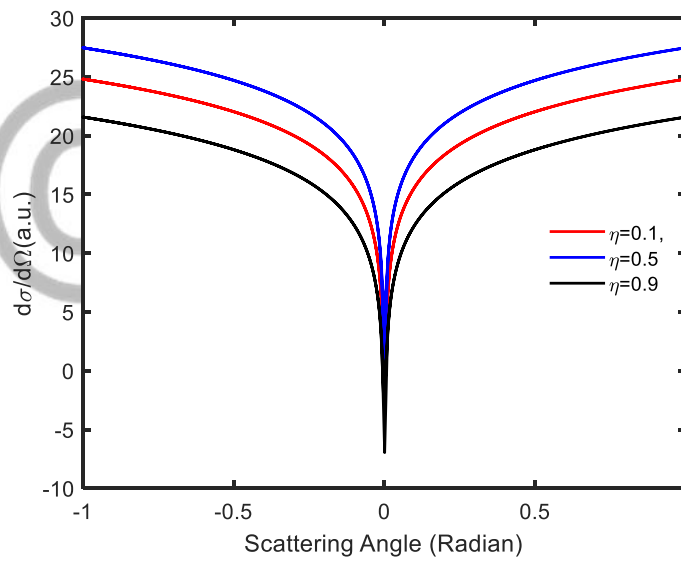
Figure 5: Scattering angle vs DCS First order Bessel function
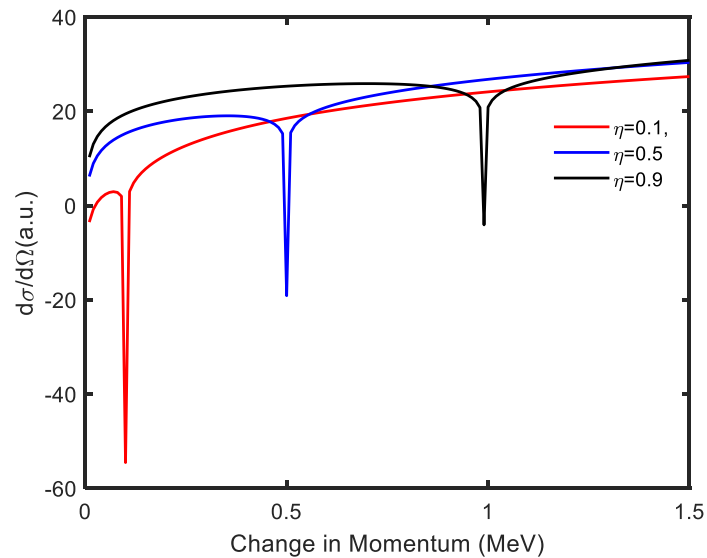
Figure 6: Change in Momentum vs DCS for First order Bessel function

Conclusion

The study investigates the Differential Cross Section (DCS) in laser-assisted electron scattering with varying parameters. Remarkably, the DCS for the first-order Bessel function surpasses the zero order, attributed to the distinctive characteristics of Bessel functions. The first order introduces amplitude modulation, leading to phase shifts and constructive interference, resulting in higher DCS values. Additionally, the interplay of screening parameters, laser field, and momentum changes significantly impacts scattering behavior. Higher screening reduces interaction, lowering DCS. Conversely, lower screening intensifies scattering, yielding higher DCS. Understanding these dynamics is pivotal for interpreting experimental results and comprehending particle behavior in this context.

References

[1] L. Treiber, B. Thaler, P. Heim, Nature Communications, 12 (2021).

[2] I. Dahiri, M. Baouahi, M. Ouali, B. Manaut, M. El Idrissi, and S. Taj, International Journal of Modern Physics B. (2023) https://doi.org/10.1142/S0217979224502898.

[3] I. Dahiri, M. Baouahi, M. Jakha, S. Mouslih, B. Manaut, and S. Taj, Chinese Journal of Physics, 77 (2022).

[4] S. El Asri, S. Mouslih, M. Ouali, S. Taj, and B. Manaut, Laser Physics, 32(2022).

[5] M. Ishikawa, K. Ishida, R. Kanya, and K.Yamanouchi, Instruments, 7(2023).

[6] M. S. Hosseini, E. Yazdani, E. Irani, B. Sajad, F. Mehradnia, S. Bazire, and A. Bayat, Optics Communications, 500(2021).

[7] X. Liu, L. Liu, M. Z. Islam, M. Gupta, W. Rozmus, M. Mandal, and Y. Y. Tsui, *Machine Learning-assisted Label-Free Cytometry Based on Laser Light Scattering of Single Cells at Multiple Wavelengths and Multiple Directions.* Optica Publishing Group, (2023).

[8] G. Buică, Physical Review A, 106(2022).

[9] K. Lévêque-Simon, and P.A. Hervieux, Physical Review A, 107(2023).

[10] S. H. Dhobi, M. D. J. Rangrej, U. Patel, N. B. Shrestha, and S. K. Sharma, International Journal of Scientific Research in Physics and Applied Sciences, 8(2020).

[11] S. H. Dhobi, S. K. Das, and Y. Yadav, European Journal of Applied Physics, 3(2021).

[12] B. Koirala, S. H. Dhobi, P. Subedi, M. Gurung, and N. K. Teemilsina, International Journal of Scientific Research in Physics and Applied Sciences, 10(2022).

[13] V. P. Filippova, S. A. Kunavin, and M. S. Pugachev, Inorganic Materials: Applied Research, 6(2015).

[14] S. Stephan, M. Thol, J. Vrabec, and H. Hasse, Journal of Chemical Information and Modeling, 59(2019).

[15] G. Buica, Journal of Physics: Conference Series, 635(2015).

[16] K. Yadav, J.J. Nakarmi, and S. Maharjan, Journal of Nepal Physical Society, 4(2017).

[17] S.H. Dhobi, K. Yadav, S.P. Gupta, J.J. Nakarmi, B. Ukrainian Journal of Physics, 67(2022).

[18] K. Yadav, S.H. Dhobi, S. Maharajan, S.P. Gupta, B. Karki, J.J. Nakarmi, Eurasian Physical Technical Journal,18(2021).

[19] B.H. Bransden, and C.J. Joachain, Physics of Atoms and Molecules. Prentice Hall, Harlow, England, 2nd, (2003).

[20] M. L. Boas, Mathematical Methods in the Physical Sciences. John Wiley & Sons, Inc, Hoboken, NJ, (2006).